AIAA JOURNAL
Vol. 44, No. 2, February 2006

Use of High-Speed Microjets for Active Separation Control in Diffusers

Vikas Kumar* and Farrukh S. Alvi†
Florida A&M University and Florida State University, Tallahassee, Florida 32310

Inlets to aircraft propulsion systems must supply flow to the compressor with minimal pressure loss, flow distortion, or unsteadiness. Flow separation in internal flows such as inlets and ducts in aircraft propulsion systems and external flows such as over aircraft wings is undesirable because it reduces the overall system performance. An experimental investigation is described that was carried out to study the feasibility of using high-speed microjets, supersonic for most cases, to control boundary-layer separation in an adverse pressure gradient. The geometry used is a simple diverging Stratford ramp equipped with arrays of 400-μm-diam microjets. Measurements include detailed surface flow visualizations, mean surface pressure distributions, and velocity field measurements using particle image velocimetry. The results clearly indicate that by activating these microjets the separated flow regions were eliminated. This led to a significant increase in the momentum of the flow near the surface where the gain in momentum was at least an order of magnitude higher than the momentum injected by the microjets. Given the simplicity of the system and its low mass flow requirements, combined with the benefits achieved by this approach, microjets appear to be promising actuators for efficient separation control for internal and external flow applications.

I. Introduction

BOUNDARY-LAYER separation entails significant energy loss, increases the flow unsteadiness, and limits the performance of many flow devices. The design of engine inlets is one area where the prevention of flow separation may be significant in improving the overall efficiency of the vehicle. Flow separation can be prevented in these engine inlets by increasing the inlet length, which generates a more gradual pressure gradient. However, the increase in the inlet length required to avoid separation and its associated losses may increase the size of the overall vehicle[1] (such as uninhabited air vehicles). In addition, for certain military applications, the inlet design is also constrained by low observability requirements. More commonly, a serpentine inlet is used to block the line of sight[2,3] to the compressor face, thereby reducing the radar signature from the compressor face. Similar "buried" propulsion systems have also been considered for the blended wing–body (BWB) design.[4]

In the case of a BWB, the engines are located at the aft end of the aircraft and, hence, require the ingestion of a thick boundary layer developed over the aircraft surface. The degraded condition of this boundary layer makes it much more susceptible to separation when it encounters the pressure gradients of a diffusing inlet duct. The pressure loss due to this separation reduces the overall system efficiency. Moreover, flow distortion and unsteadiness created due to this separation can also result in aerodynamic stall and a surge in the compressor and fan blades.[5,6] Consequently, it is highly desirable to avoid boundary-layer separation in inlets because it can significantly diminish the engine performance.

Not surprisingly, a substantial amount of research aimed at controlling boundary-layer separation[7,8] has been conducted. Conventionally, the following approaches have been applied for separation control: 1) tangential blowing to energize directly the low-momentum region near the wall,[9–11] 2) wall suction[12,13] to remove the low-momentum region, 3) vortex generators (VGs and micro VGs) in the form of vanes and bumps,[14,15] and 4) forced excitation devices, for example, acoustic excitation[16,17] and synthetic jets.[18,19] Tangential blowing and suction are very effective in controlling separation. However, they have the parasitic cost involving high-pressure (mass flux) sources and are infrequently used. VGs are among the most widely examined flow control methods, where VGs of various shapes and sizes have been used to control boundary-layer separation.[15] Although the mechanism is still not well understood, it has been suggested that the VGs produce strong vortices, which enhance the mixing between the high-momentum core flow and the low-momentum boundary-layer flow, thus energizing the boundary-layer fluid.[1] However, the performance of these VGs, which are passive in nature, has been somewhat limited; usually there is a need to optimize their location, size, and other parameters to achieve optimal performance for specific operating conditions. In addition, they have an associated parasitic drag when they are not in use.

An excellent review of active flow control techniques has been published by Greenblatt and Wygnanski.[20] As discussed in their review of the use of acoustic excitation methods for separation control (over airfoils) (Sec. 3.2 in Ref. 20), they note that certain methods, such as those used by Ahuja et al.[17] and Zaman et al.[16] have shown some benefits. However, these acoustic excitation studies were in most cases facility dependant and, therefore, perhaps of limited use from a practical perspective. To quote Greenblatt and Wygnanski "The drawbacks, however, outweigh these positive aspects." Other active flow control devices, such as synthetic jets,[18] have also been examined for separation control applications. Amitay et al.[18] demonstrate that their synthetic jet-based actuators provided some control of flow separation in a duct. The measurements by Amitay et al. consisted of pitot surveys that showed that flow attachment was generally obtained for a limited region of the flowfield and that complete reattachment was limited to a few cases. Similar flow control devices have been employed by Jenkins et al.,[19] who employed piezoelectric-synthetic jets to control flow separation over an adverse pressure gradient ramp essentially identical to the one used in the present study. Based on their results, Jenkins et al. concluded that their synthetic jets did not work, primarily due to the "insufficient velocity/momentum output" that is needed to achieve effective control.

A different approach, one that employs microjets to control flow separation, is presented in this paper. In this study, we plan to investigate the efficacy of using high-speed microjets (supersonic

Presented as Paper 2003-4160 at the AIAA 33rd Fluid Dynamics Conference, Orlando, FL, 23–26 June 2003; received 24 February 2004; revision received 9 July 2005; accepted for publication 13 July 2005.

*Graduate Research Assistant, Department of Mechanical Engineering, 2525 Pottsdamer Street. Student Member AIAA.

†Associate Professor, Department of Mechanical Engineering, 2525 Pottsdamer Street. Senior Member AIAA.

for most applications) to control flow separation. Based on their success in other applications[21] and that supersonic microjets provide a unique combination of high-momentum and low-mass flow rates, we anticipated that these active flow control devices may also be effective in separation control. It is well known that jets in crossflow, which is in essence the flow generated by the actuation of microjets, can generate longitudinal streamwise vortices[22] in a boundary layer. These vortices, in turn, appear to increase cross-stream mixing, thus increasing the streamwise momentum of the near-wall fluid. It was our expectation that in a manner similar to solid VGs (but perhaps more efficiently), high-speed microjets would, thus, energize the boundary-layer fluid by creating strong streamwise vorticity,[23] thereby enhancing mixing with the more energetic flow. Furthermore, due to their small size, relative simplicity, and ease of implementation, if successful, engine inlets or other flow surfaces, such as airfoils, can be relatively easily populated with these microjets.

II. Experimental Details

A. Facility and Model

The experiments were conducted in a subsonic, closed-return wind tunnel with a maximum freestream velocity of 60 m/s in the 48×24 in. test section. The diffusing duct flow is powered by a radial blower that passes through a settling chamber before entering the test section. Honeycomb screens in the settling chamber ensure flow uniformity. The contraction then accelerates the flow from the settling chamber into the test section, further reducing flow perturbations. A pitot static probe was used to measure the flow speed in the test section.

The geometry used for the test model is a simple adverse pressure gradient ramp, similar to the model used at the NASA Langley Research Center for examining the effectiveness of various control techniques.[19] In theory, the ramp profile produces a Stratford-like pressure gradient[24] in the test section. This model, mounted in the wind tunnel, is shown in Fig. 1. Note that a Stratford pressure profile is theoretically expected to lead to an incipiently separated flowfield where the separated flow region, if any, would be very small. However, as our results will indicate, the size of the separated flowfield that was actually obtained and subsequently controlled using microjets was significantly larger. The Stratford criterion is an approximate one, and, in many experiments, the flow separation occurs much earlier than predicted using this approach.[25] Suffice it to say that the flow regimes where microjet efficacy is evaluated is not incipiently separated, and, as noted near the end of this paper, in recent ongoing experiments we have been able to eliminate separated flow regions that are significantly larger than those discussed here.

The ramp is equipped with approximately 50 surface static pressure ports to obtain the mean surface pressure distributions. These pressure ports were placed along the model centerline, as well as in transverse rows at selected locations. The pressure coefficient C_p is then determined using the conventional definition

$$C_p = \frac{(P_s - P_\infty)}{0.5\rho U_\infty^2}$$

where P_s is surface static pressure and P_∞ is the freestream pressure.

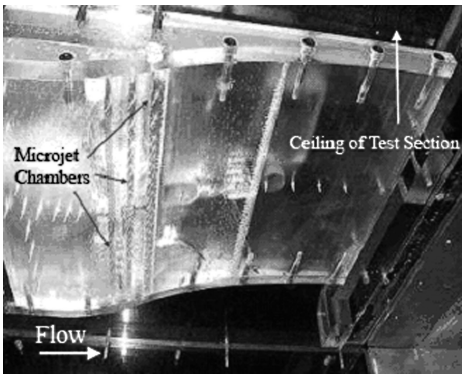

Fig. 1 Ramp model, mounted in wind tunnel.

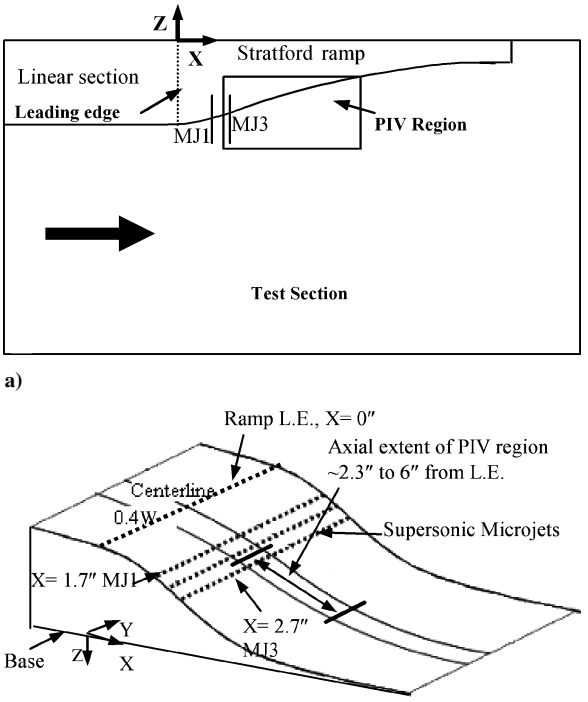

Fig. 2 Schematics: a) test section and b) ramp model.

A schematic of the test section is also shown in Fig. 2a. As seen in Figs. 2a and 1, the ramp is mounted on the top of the test section, and the flow is from left to right. A detailed schematic of the ramp model is also shown in Fig. 2b. As shown in Fig. 2b, the ramp, that is, the surface divergence, begins at $X = 0$ in. and is preceded by a flat section of 21.5 in. in length. Figure 2b also indicates the region where the particle image velocimetry (PIV) measurements, discussed later in this paper, were obtained. PIV data were obtained at three streamwise planes, along the centerline, $0.1W$ and $0.2W$ away from the centerline, where W is the width of the ramp. Only the centerline and the $0.1W$ plane are shown in Fig. 2a to give an idea of its location. This off-centerline plane is referred to as the $0.4W$ location. PIV results from the centerline plane and the $0.4W$ are discussed in this paper, the reasons for which are discussed later.

Also shown in the Fig. 2a are the locations of microjet arrays, where each array consists of about 60 microjets, 400 μm in diameter. These microjets were oriented vertically, that is, 90 deg with respect to the freestream. The spacing between these microjets was 5.6 mm. The diameter of these microjets was chosen to be 400 μm because this represented a good compromise between small size and minimal viscous losses that increase significantly as one employs smaller jets. The microjet flow becomes supersonic when the stagnation pressure exceeds ~13 psig. Because most of the test cases presented here are for a stagnation pressure of 25 psig, they are often referred to as supersonic microjets. Flow through nozzles of this diameter has been previously examined,[26] and similar actuators have been used in other applications, such as impinging jets.[21] This was another reason for using microjets of this specific size.

Note that the results discussed in this paper correspond to the use of first and third microjet arrays for separation control. The placement of these microjets with respect to separation location is expected to be a critical parameter for the control scheme. It was also anticipated that the actuators should be placed upstream of the separation zone for optimal effect. Because the exact location of the separation was not known, the microjets were placed upstream of the region where separation was observed in the study by Jenkins et al.[19] Gas for these microjets was supplied from high-pressure nitrogen tanks, where exhaust pressure was being controlled by a regulator. Nitrogen was used because it is easily available in pure form and has gasdynamic properties that are very similar to air.

B. Measurement Techniques

Both qualitative and quantitative measurements were obtained to gain a better understanding of the overall flowfield behavior. Mean surface static pressure measurements were first obtained by sequentially scanning surface pressure taps, suitably distributed over the ramp surface. The pressures were scanned using a 48-channel scanivalve unit, which in turn was connected to a pressure transducer. All pressure transducers were frequently calibrated and checked for drift. The data were sampled and recorded using personal-computer-based National Instruments Data acquisition hardware and software. An average of 4000 samples was acquired to obtain a reliable estimate of the mean surface pressures.

The topographic nature of the surface flowfield was also examined using a surface flow visualization technique. This was achieved by applying water-based paint on the surface of the ramp. The painted model was then exposed to the flow to obtain the surface flow pattern. The flowfield above the surface was also quantitatively studied using the two-dimensional PIV technique. The test section was seeded with smoke particles, approximately 5 μm in diameter, using a Rosco fog generator. A New Wave^{TM} Nd-YAG pulsed laser with a repetition rate of 15 Hz was used to illuminate the particles introduced into the flowfield. Each PIV image pair was then acquired using a Kodak ES 1.0 high-resolution charge-coupled device camera capable of recording 10-bit digital image pairs in separate frames at a rate of 15 image pairs/s. Further details of this PIV technique can be found in Ref. 27. One of the main advantages of this PIV technique is a novel processing scheme with high spatial resolution that uses image matching to extract the particle displacements and, hence, the velocities, from particle image pairs.[28]

C. Test Conditions

The experiments were conducted over a range of freestream velocities from 10 to 50 m/s. For all of these freestream velocities, various combinations of microjet locations and pressures were investigated. Separation was completely eliminated for the highest freestream velocity tested in the facility by the proper combination of microjet pressure and location. However, for the sake of brevity, results discussed here are mainly limited to the 40-m/s case because it illustrates the principal flow features and its response to microjet control. Also, the effect of microjet control presented here will primarily be limited to the actuation of the third microjet array (MJ3), with selected results shown for the first microjet array (MJ1). While conducting these experiments, we were cognizant that any active flow control technique in a practical system should not require more than 1% of the inlet mass flow.[29] This actuator mass flow limit is expected to minimize the adverse impact of an active flow control system on the overall vehicle. With these restrictions in mind, the microjets were pressurized up to a stagnation pressure of 25 psig. Under the assumption that the boundary layer in the present experiments occurs in a 30% boundary-layer ingesting duct, the nominal value used for a BWB inlet,[29] the 25-psig microjet pressure roughly corresponds to 0.5% of the inlet mass flow in such a duct. This is well below the 1% threshold. Although the effect of microjet on the flow was evaluated over a range of pressures (Table 1), the microjet stagnation pressure of 25 psig has been used in this paper as the primary test case at which to demonstrate and discuss the effect of microjet control. This is in part due to this also being the pressure where separation was eliminated with minimal mass flux for the worst-case scenarios, for example, maximum freestream velocity and actuators farthest away from the separation location.

Table 1 Momentum injected vs momentum gain achieved for various microjet pressures

Microjet activated	Microjet Pressure	C_μ, %	MGR
MJ1	10	11.76	13.22
MJ1	15	19.58	9.53
MJ1	20	29.06	4.71
MJ1	25	39.71	7.44
MJ3	10	11.76	49.61
MJ3	15	19.58	40.38
MJ3	20	29.06	33.56
MJ3	25	39.71	28.78

The Reynolds number at the ramp leading edge at 40 m/s is 1.3×10^6. At this velocity, the boundary-layer thickness δ was measured at the leading edge of the ramp at the centerline (using a boundary-layer pitot probe) and was found to be 0.75 in. The boundary-layer profile was in close agreement with a seventh power law profile indicating that the incoming boundary layer is nominally turbulent. Under these conditions, the corresponding displacement thickness δ^* and the momentum thickness θ at the ramp leading edge were estimated to be 0.12 and 0.08 in., respectively.

III. Results and Discussion

A. Baseline Case: No Control

1. *Surface Properties*

Figure 3 shows a comparison between the measured C_p distributions for the baseline, uncontrolled flow at 40 m/s and the flow with microjet control, where MJ1 has been activated at 25 psig. As shown in Fig. 3, C_p values have been plotted on a reverse scale on the y axis. For reference, the ramp geometry is also included, where the ramp height is indicated on the y axis on the right and the location of MJ1 and the last array of microjets is shown in dashed lines. The repeatability of these experiments was checked over a period of 4 months, and the results were found to be repeatable within 1%. It is observed that, upstream of the microjet location, the baseline and the microjet control cases show a similar pressure distribution. Downstream of the microjet location, however, the pressure distributions differ, the pressure recovery being higher for the control case. Similar observations for C_p distributions were made by Lin[15] in his study of separation control using passive control devices. Although the pressure recovery is improved with microjet control, the improvement does not seem to be substantial. As the following results will show, this may partially be because for this case the size of the separation is somewhat limited. Hence, the pressure loss will be correspondingly small resulting in a corresponding small recovery when separation is eliminated. Pressure distribution along the centerline, however, provides only limited insight into the flow behavior, and, based on C_p distribution alone, it is difficult to determine conclusively whether the effect of microjets is beneficial and to what extent.

The surface flowfield was then shown to further characterize the nature of the separation region on the model. In general, the surface flow streamlines are skin-friction lines because they are formed under the influence of wall shear stresses rather than pressure gradients. However, this is not true for reverse flow regions where the surface shear stress is very small and where the motion is a result of both shear stress and pressure gradient. As such, the lines of separation indicated by the flow pattern are normally ahead of the actual separation location.[30] The surface streamline pattern for flow without

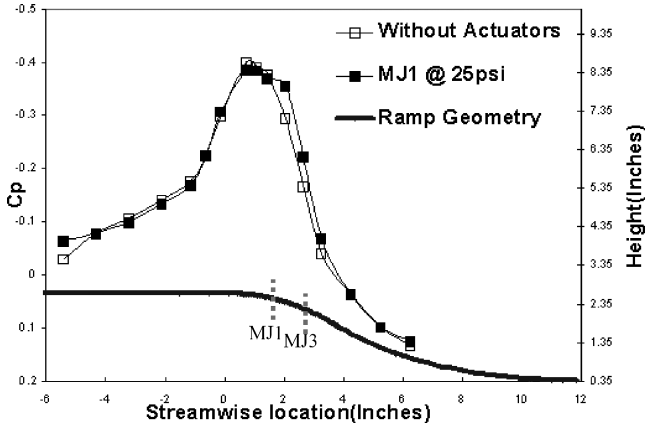

Fig. 3 C_p distribution along centerline at 40 m/s, with and without microjets.

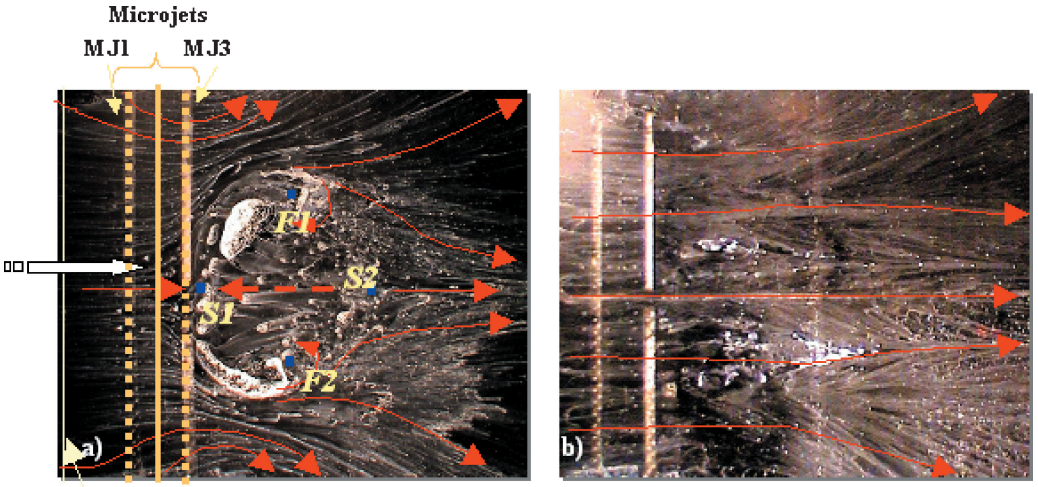

Fig. 4 Surface flow traces at 40 m/s: a) no control, $x/L = 0$ and b) MJ3 at 25 psig, $x/L = 1$.

control is shown in Fig. 4a. Also in Fig. 4a are the streamlines indicating the flow direction. These streamlines have been drawn based on the visual observations during the experiment. The flow pattern obtained is very similar to the "Owl Face" pattern of the first kind.[31]

The horizontal streamlines in the upstream, left half of Fig. 4a indicate that the flowfield is fairly uniform and relatively two-dimensional in this region. However, three-dimensional effects can be observed immediately downstream of the ramp leading edge. The secondary flow near the ramp edges (Fig. 4a) also appears just downstream of the location where the ramp begins. This secondary flow may in part be due to corner vortices generated at the edges of the model; however, its exact nature and its effect, if any, on flow separation is not clear at this point.

The reverse or separated flow region is also indicated in Fig. 4a. The surface streamlines emanating from the front stagnation point (S1, Fig. 4a). Form a separation bubble, which ultimately spirals around two focal points F1 and F2 (Fig. 4a). These focal points are also the points of local pressure minima. The streamlines then reattach at S2 (Fig. 4a). In essence, the surface flow pattern shows a trapped separation bubble, generated due to the ramp curvature, and this separation bubble appears to be "kidney" shaped.[31] Consequently, to verify the shape of the separation bubble above the surface, PIV measurements were subsequently obtained along the centerline plane and at two planes away from the centerline, as described in Sec. II.A. Only velocity-field data for the centerline plane (Fig. 2b) have been presented here for the sake of brevity. The effect of flow control on the surface flow pattern, shown in Fig. 4b, will be discussed in a subsequent section.

2. *Velocity Field Measurements*

A typical processed instantaneous velocity vector field for the no-control case, obtained using the PIV technique, is shown in Fig. 5a. Smoke was introduced from the surface ports in the upstream section of the model, and the entrained particles were shown using a thin laser sheet generated using an Nd-YAG laser. A significant reverse flow region is clearly evident. A discussion of the flowfield with microjets activated at 25 psig, shown in Fig. 5b, will be delayed until the effect of control is discussed later in the paper. For a better understanding of the separation region and the effect of microjet control, mean flow properties are presented next.

Figure 6a show the streamwise component U of the mean velocity field in the centerline plane, corresponding to a freestream velocity of 40 m/s. Note that in these and all subsequent PIV data included in this paper, the ramp model is at the top of figures, the freestream flow is from left to right, and the microjets issue from the top. The inset in Fig. 6a shows the ramp geometry and the region where the PIV data were obtained. In all of the plots shown in this paper, all distances have been normalized with respect to the

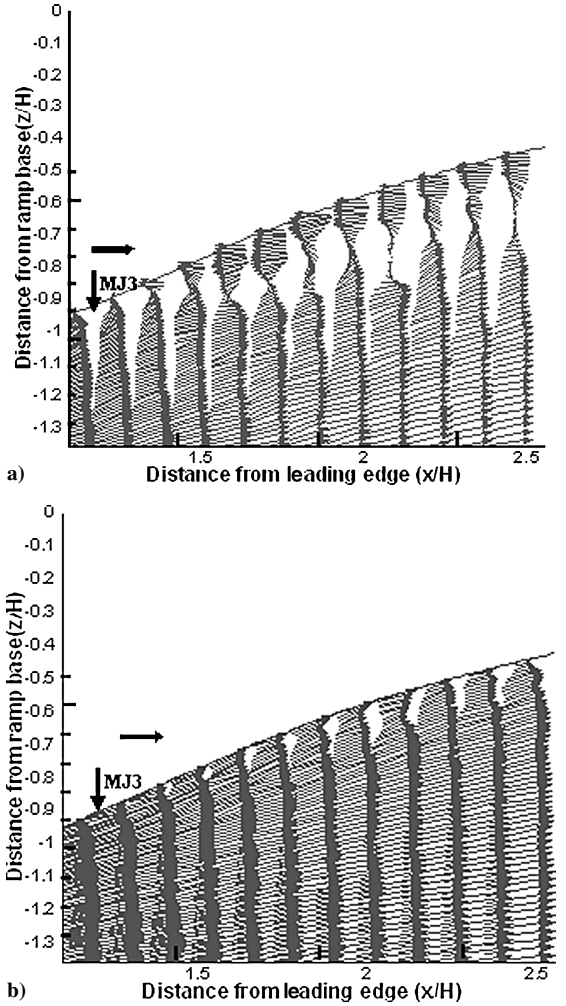

Fig. 5 Processed velocity vectors: a) no control at 40m/s and b) MJ3 at 25 psig at 40 m/s.

ramp height. The y axis represents the vertical distance from the base of the ramp, and the x axis is the streamwise distance from the ramp leading edge. (Refer to Fig. 2a for the origin of the coordinate frame.)

A closer look at Fig. 6a shows that as one proceeds downstream in the vicinity of the surface, there is a rapid deceleration in the fluid velocity, which eventually leads to a region of reverse flow. This reverse flow zone corresponds to the dark blue velocity contours (Fig. 6a)

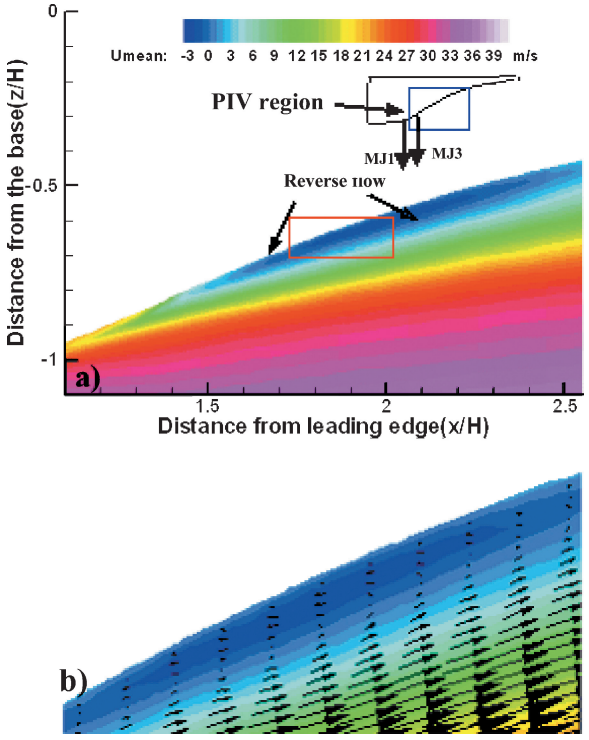

Fig. 6 Velocity field for 40m/s, no control: a) streamwise velocity component U and b) velocity vector for region indicated in Fig. 6a.

and starts at approximately $x/H = 1.6$ and ends at approximately $x/H = 2.2$ (corresponding to a physical length of approximately 2 in.). A small subregion of this flowfield, roughly indicated by the box in Fig. 6a, has been magnified in Fig. 6b, which shows the velocity vectors. The presence of reverse flow, close to the ramp surface, is clearly visible in Fig. 6b, indicating that the flow has separated locally resulting in a separation bubble with recirculating flow. Although not included in this paper for the sake of brevity, the presence of reverse flow was further confirmed by examining the vertical component of the velocity (perpendicular to freestream). Contour plots of this velocity component clearly reveal the presence of low-magnitude velocity fluid moving away from the boundary in the same region where the reverse flowfield is seen in the streamwise velocity components. As noted by other researchers (see Ref. 15), it was also observed that increasing the freestream velocity causes the flow to separate further upstream, whereas the flow attachment location does not change appreciably, leading to a larger separation region. Though these results are not included here, freestream velocities up to 65 m/s were examined, resulting in much larger separation zones than the 40-m/s case discussed in this paper. These larger separated flows were subsequently controlled using microjets.

As noted earlier in the discussion of the surface flow traces (Sec. III.A.1) this separation appears to be three-dimensional in nature. Hence, ideally, one would like to obtain velocity measurements in planes perpendicular to the freestream flow, that is, in the Y–Z plane (Fig. 2b); such measurements are planned in future experiments. At present, PIV measurements were obtained at three off-centerline axial planes to provide some insight into the three-dimensional effects. Although not shown here, a comparison to the centerline velocity field (Fig. 6a) reveals that as one moves away from the centerline plane, the size of the bubble grows appreciably larger (at the $0.4W$ plane) and then reduces as one approach the sides of the ramp. This result is consistent with our earlier observation based on the surface flow pattern, that the separation bubble is kidney shaped and is, therefore, expected to be smaller in the central plane.

To summarize, the surface flow and flowfield measurements clearly reveal that the adverse pressure gradient along the ramp leads to a significant local separation of the incoming boundary layer where this separation region is three-dimensional in nature. In the following subsection, we examine effect of applying flow control using supersonic microjets on this separated flowfield.

B. Effect of Microjet Control

Qualitative visualizations of the flowfield indicated that when the microjets were turned on at the appropriate pressure, the reverse flow or the separated flow region is eliminated. These observations were confirmed with the PIV results, to be discussed later. Significantly, this effect of microjet control was observed for all of the conditions where separated flow was present for the baseline case.

1. *Surface Properties*

We begin with the discussion of the surface flow visualization, shown in Fig. 4b, which reveals the effect of microjets on the surface flow pattern. As seen in this surface flow trace, no regions of reverse velocity are visible. The flow pattern, however, is not completely two-dimensional, and three-dimensional features, such as diverging streamlines, can be seen. As discussed later, it is anticipated that one of the mechanisms at work in the present control technique is the introduction of streamwise vorticity by the microjets. As such, one may argue that some of the features in Fig. 4b are similar to footprints of streamwise vortices. However, at present, the exact nature of these features is not clear. What is clear is that the microjets eliminate the large separation bubble seen in Fig. 4a. In the following sections, we examine the flowfield in further detail using the velocity field measurements to better quantify the effect of microjets on the separated flows.

2. *Velocity Field Measurements*

The visual effect of the microjets can be seen from the instantaneous velocity vector field in Fig. 5b, obtained using PIV. The image was obtained with MJ3, operating at 25 psig. A comparison with Fig. 5a clearly shows that not only has the reverse velocity zone been eliminated, but there has also been a significant momentum addition along the surface. To study this effect of microjets, the influence of various parameters on separation control was examined, as described next.

The first parameter considered was the freestream velocity. Figure 7a shows the streamwise velocity data for the centerline

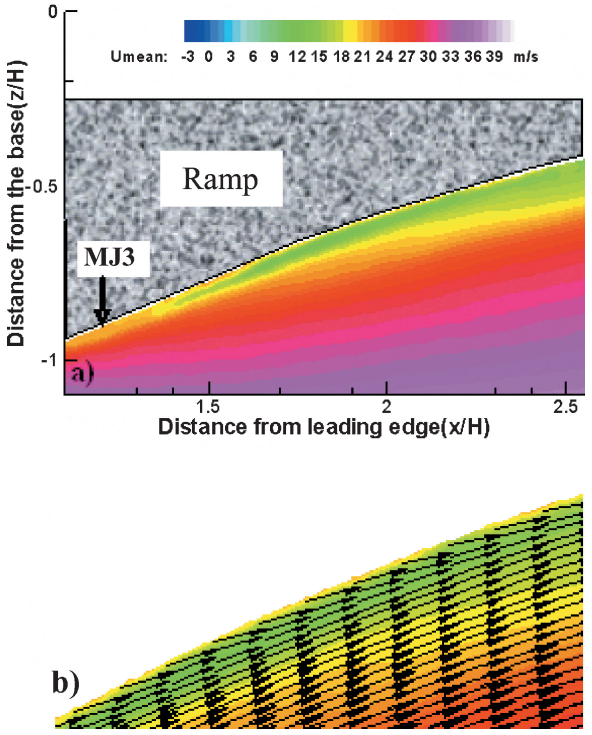

Fig. 7 Velocity field for 40m/s, MJ3 at 25 psig: a) streamwise velocity component U and b) velocity vector for region indicated in Fig. 7a.

plane at 40 m/s, where MJ3 is operating at 25 psig. A comparison of Fig. 7a with Fig. 6a shows that the activation of microjets completely eliminates the reverse flow region; very similar effects were also observed for the 50-m/s case, where the separated flowfield was 15–20% larger. Also note that, at 40 m/s, the velocity measured with control near the surface was somewhat higher than for the 50-m/s case. This suggests that the ratio of the microjet momentum relative to the freestream momentum may be an important parameter. This effect of the momentum flux ratio is, of course, well known and has been discussed by numerous other investigators.[20]

To quantify the efficacy of microjet control in terms of the mass and momentum flux supplied by the microjets, the mass flux coefficient M^* and the steady momentum coefficient C_μ were defined as follows: M^* is the mass flux of the microjets divided by the mass deficit based on δ, where δ is the boundary-layer thickness at the ramp leading edge.

The mass flow rate m_{in} through the supersonic microjets can be conservatively estimated by assuming choked flow through the micronozzles. The mass coefficient is then given as

$$M^* = m_{\text{in}}/\rho_\infty U_\infty y\delta$$

where ρ_∞ is the freestream density, U_∞ is the freestream velocity, and y is the span of the ramp.

The momentum flux ratio is given by the conventional definition of the steady momentum coefficient[20] and is given as

$$C_\mu = \frac{N m_{\text{in}} U_j}{\frac{1}{2}\rho_\infty U_\infty^2 y\delta}$$

where N is the number of microjets and U_j is the jet velocity.

Thus, C_μ is the ratio of the magnitude of the total momentum injected into the flow relative to the freestream dynamic pressure multiplied by an appropriate area, chosen as δy in the present case. These values of C_μ and M^* for various microjet operating pressures are shown in Fig. 8. As expected, C_μ and M^* are related such that small increments in M^* yield progressively larger C_μ, thus accounting for the effectiveness of microjets with relatively little mass flow injection. Measurements show that increasing the microjet operation pressures, that is, increasing the C_μ, results in higher velocities closer to the ramp surface, indicating the presence of higher momentum in the near-wall region. The reason behind this behavior may be due to one or more of the following as C_μ increases: 1) More momentum is directly injected into the boundary layer. 2) Strong streamwise vortices[22] are generated that enhance mixing with the outer, high-momentum fluid. 3) The microjet jet momentum and penetration depth[32] increases, enhancing the transfer of momentum from the freestream fluid to the boundary-layer fluid (E. R. Norster, "Jet Penetration and Mixing Studies," unpublished work, College of Aeronautics, Cranfield University, Cranfield, England, United Kingdom; see Ref. 32).

A magnified view of a selected region for the 40-m/s case (Fig. 7a) is shown in Fig. 7b, in the form of a velocity vector plot. A comparison with Fig. 6b shows that with the activation of microjets, velocity

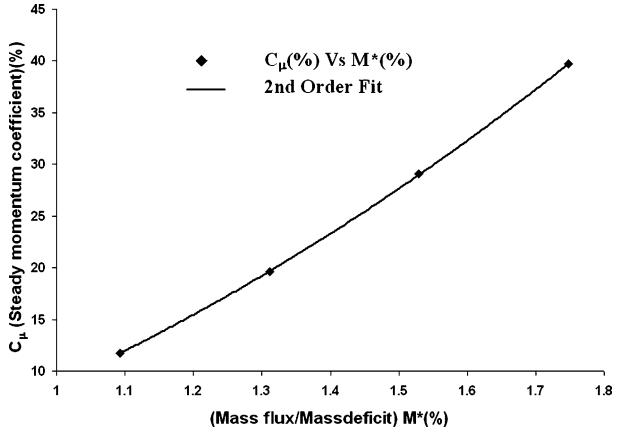

Fig. 8 Steady momentum coefficient C_μ vs. mass flux coefficient M^*.

vectors in the zone previously corresponding to reverse flow now possess significant momentum in the forward direction. At 25 psig, the mass flux supplied by the microjets is approximately 1.7% of the mass flux across the ramp, based on the boundary-layer thickness, that is, $M^* = 0.017$. This pressure corresponds to a C_μ of 0.397, or 39.7%, which amounts to a C_μ of 6.3*e*-03/jet, which is much higher than the 2*e*-03/jet value quoted by Amitay et al.[18]

In general, any separation control input must be applied at or close to the separation point. To investigate the effect of the actuator location, experiments were conducted with microjets at different axial locations along the ramp. The microjets were successful in eliminating the reverse flow region regardless of their location. However, on comparison of the effect of MJ1 with the results shown in Fig. 7a for MJ3, it appears that, although both microjet arrays were able to eliminate separation, higher velocities closer to the surface were obtained with the activation of MJ3. In addition, the reverse flow region was eliminated with a lower momentum flux input using MJ3 compared to MJ1, indicating that, as expected, choosing an appropriate location to apply flow control is an important parameter for optimal flow control.

Whether the microjets eliminate the entire three-dimensional separation region was also examined using the PIV results acquired at the off-centerline locations. Although separation was completely eliminated, it was noticed that the effect of control was not as pronounced as in the centerline plane. For example, the magnitude of the U component of the velocity near the ramp surface was somewhat less than the velocities measured along the centerline. The reasons for this are attributed to the three-dimensional nature of the separation bubble and perhaps also due to the presence of secondary corner flow as discussed in Sec. III.A.1. Although the details of the effect of microjets at off-centerline locations are not completely understood at present, there is no doubt that, overall, they have a beneficial effect in that the microjets eliminate or significantly reduce the size of the separation region. An examination of the three-dimensional effects is the main focus of ongoing research at our laboratory.

3. Closer Look at Control Effects and Mechanisms

To determine whether the significant increase in the momentum near the ramp surface is simply due to the direct injection of momentum by the microjets, we define a parameter referred to as the momentum gain ratio (MGR). It is the ratio of the increase in momentum due to microjet control relative to the momentum injected by the microjets. Hence, the MGR is given as

$$MGR = \frac{\text{momentum}_{\text{with control}} - \text{momentum}_{\text{no control}}}{\text{momentum}_{\text{microjets}}}$$

$$= \frac{\int(\rho U\,\mathrm{d}A)_{\text{with control}} - \int(\rho U\,\mathrm{d}A)_{\text{no control}}}{N\dot{m}_{\text{in}} U_j}$$

The momentum flux with and without control was calculated at axial locations by numerically integrating the velocity field data. A comparison of the momentum gain achieved with the application of different microjets at various operating pressures is listed in Table 1 and shown in Fig. 9. Both the tabulated results and Fig. 9 clearly show that, for the same C_μ values, the momentum gain achieved with MJ3 is significantly more than that achieved with MJ1. In particular, at 25 psig, the momentum gain with MJ1 is 7.8, whereas the momentum gain achieved with MJ3 is 30. This reaffirms the notion that the location of the actuators relative to the separation location plays a very important role in the efficacy of control. Furthermore, it suggests that the closer one is to the separation location, the more effective control can be achieved.

This high MGR clearly indicates that some other mechanism(s), distinct from direct injection of momentum, plays an important role in this control approach. As mentioned earlier, one of the physical mechanisms we expect to be of significance is the generation of streamwise vorticity by the supersonic microjets.[22,33] This streamwise vorticity is expected to enhance the entrainment of the freestream fluid into the boundary layer. In addition, it may also promote mixing between the low-momentum portions of the boundary

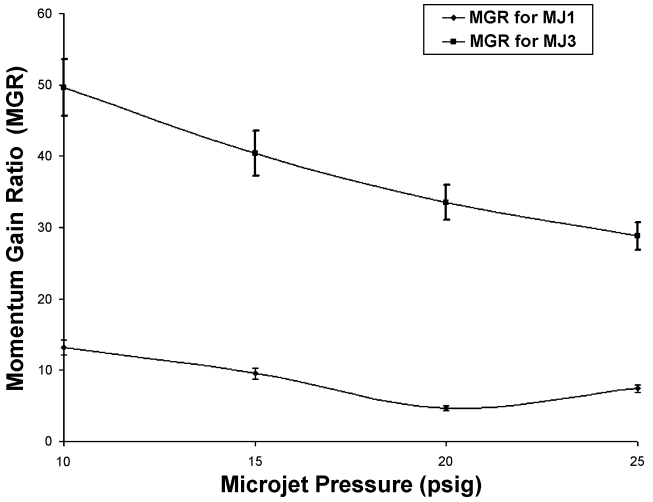

Fig. 9 Effect of microjet location on MGR.

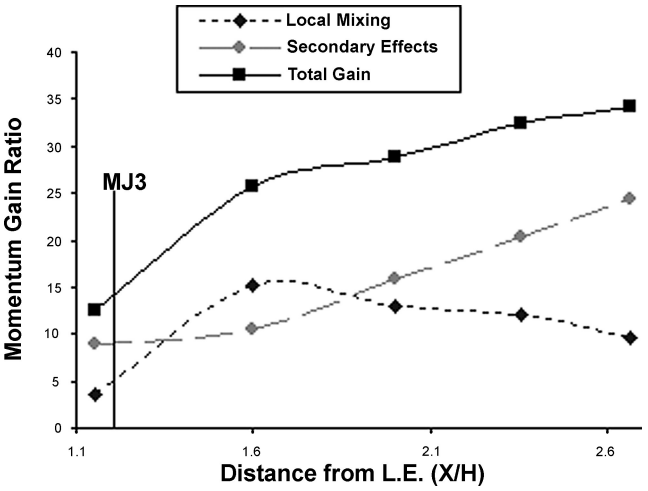

Fig. 10 Comparative view of microjet effects, MJ3 at 25 psig.

layer, very close to the surface, with the higher-momentum fluid away from the wall, thus, preventing or delaying separation.

To further explore and understand the effect of the microjets, we sought to delineate the effects of flow control on the MGR into two regions, as follows. We first identify a region where the near-wall fluid directly encounters the microjets and define its extent as the maximum penetration depth of the microjets. Hence, this defines the zone in which the microjets may influence the local flow directly. The second zone is the remainder of the boundary-layer flow outside the area of direct influence. In this second zone, the gain in momentum due to flow control may be more strongly influenced by other mechanisms, such as the generation of streamwise vorticity, physical mechanisms that we collectively refer to as the secondary effects of the microjets. As documented by others,[22,34] the penetration depth of jets in a crossflow is mainly a function of the momentum ratio. Although there are a number of primarily empirical correlations available in the literature for estimating the penetration of jets in crossflow, for the present analysis, the maximum jet penetration $Y_{\max}$ of a single jet into a duct with a crossflow was evaluated using Norster's equation (E. R. Norster, unpublished work; see Ref. 32):

$$Y_{\max}/d_j = 1.15 \times \left(\rho_j U_j^2 \big/ \rho_\infty U_\infty^2\right)^{0.5} \times \sin(\delta_j)$$

where ρ_j is the jet density, d_j is the jet diameter, and δ_j is the microjet blowing angle at the vena contracta.

By the use of the preceding correlation, the penetration of the microjets was determined to be approximately 0.2 in., almost one-quarter of the boundary-layer thickness. This leads to the definition of the region of direct influence as that below this one-quarter boundary-layer plane, $\delta_{0.25}$. Outside $\delta_{0.25}$, one would expect the gain in momentum to be due to the secondary effects, as discussed earlier. With these definitions, the MGR for MJ3 operating at 25 psig is evaluated at various axial locations for both the direct and secondary effects, and the results are shown in Fig. 10. Figure 10 shows that downstream of the microjet injection location, the direct effect initially starts to grow rapidly. This initial rapid growth of the direct effect zone occurs in the vicinity of the microjet injection location, a region generally identified as that where the initial evolution, penetration into and turning due to the freestream flow, occurs.[35,36] Further downstream, the momentum gain due to the direct effects appears to saturate and even decline. However, the contribution of the secondary effects continues to grow downstream of the injection location and plays a proportionally larger role as one moves downstream. This suggests that the secondary effects, which we suspect to be due to the generation of streamwise vorticity, continue to energize the boundary-layer flow by entraining high-momentum fluid from the freestream.

We recognize that there are many ways in which one can examine the results obtained in our study to better elucidate the flow physics behind this control technique; the preceding analysis and discussion is one simple, phenomenological-based attempt to do so. This is an issue that we are continuing to study further and in more detail and hope to gain a better understanding of through additional experiments and analysis. However, it is clear at this point that the present control technique is not effective simply due to the direct injection of momentum into the boundary layer of fluid.

Finally, we briefly examine the effect of microjets on the flow unsteadiness. Figure 11a and 11b present the fluctuating component of the streamwise velocity U_{rms} for the uncontrolled and the controlled cases, respectively. As before, these results correspond to a freestream velocity of 40 m/s where MJ3 was activated at 25 psig for the controlled case. In Fig. 11 U_{rms} has been nondimensionalized with the freestream velocity. A comparison of Fig. 11a with Fig. 11b shows that the velocity fluctuations associated with the flow have been dramatically reduced, by as much as 50% or more. In fact, most of the regions associated with high fluctuations have disappeared. Not only have the velocity fluctuations been reduced in magnitude, but also the regions in which these fluctuations occur have become much smaller. Although not shown here, a comparison of turbulence kinetic energy associated with uncontrolled cases was also made.[37] It was observed that the level of turbulence associated with the flow was also reduced by almost 50%; similar effects were observed at higher freestream velocities.

To summarize, although the physical mechanisms behind microjet control still need to be explored further, based on the use of microjets in other applications[21,23,34] and on our present results, it appears that the streamwise vorticity due to the microjets may play a primary role in this control approach. The generation of streamwise vorticity can be due to a number of mechanisms. First, the microjets may behave as fluidic tabs, much like the micro-VGs used in earlier work.[14,15,19] Second, the vorticity in the microjets is redirected in the streamwise direction by the mean flow, and, finally, the microjets may also redirect the spanwise vorticity in the base flow in the streamwise direction by vorticity tilting. These mechanisms may be similar to those discussed by Alvi et al.[33] in the context of impinging jet control using microjets.

Finally, we note that in more recent, ongoing experiments, we have been able to increase the freestream velocity to 65 m/s. This, together with a more aggressive ramp geometry, has allowed us to generate separated flow regions that are much larger (two to three times larger) than the cases presented here. With the proper use of microjets, we have been able to completely control, that is, eliminate, these more challenging separated flows, providing further evidence of the potential utility of this control approach. We have also been able to reduce the mass flow rates required to eliminate this separation by 40%. This work is ongoing, and additional, more detailed measurements are planned to shed more light on the physics behind this control mechanism. The effect of microjet location, microjet angle, as well an examination of the flowfield in the cross plane

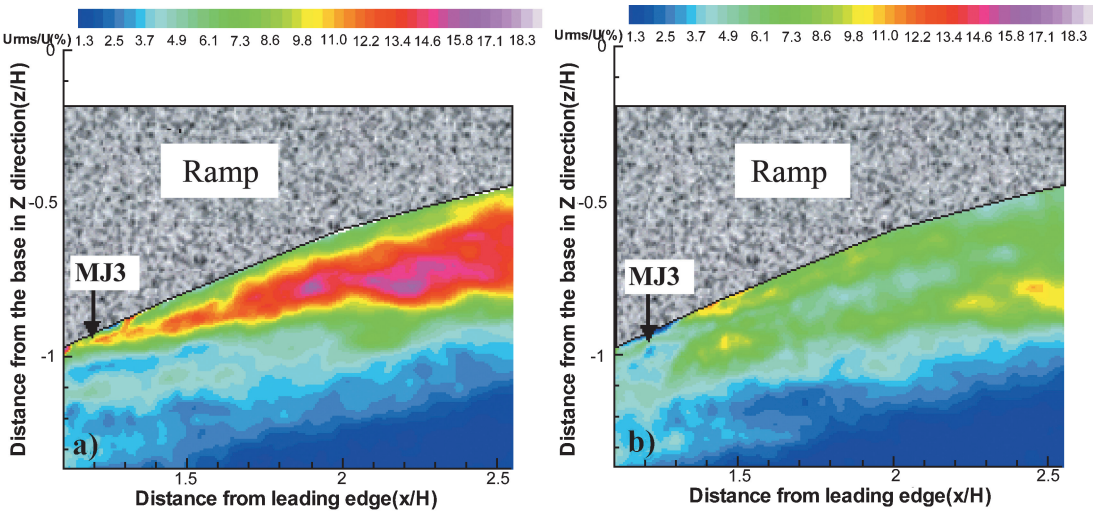

Fig. 11 $U_{\rm rms}$ **velocity: a) no control and b) MJ3 at 25 psig.**

are some areas that require further exploration to better understand the mechanism for flow control. Future experiments are planned to address some of these issues.

IV. Conclusions

A study of separation control in an adverse pressure gradient region over a Stratford ramp[24] has been performed. Separation control was implemented using strategically placed arrays of high-speed/supersonic microjets. These results, which consist of surface pressure distributions, surface flow visualizations, and velocity-field measurements, indicate that the microjets have an appreciable and desirable effect on flow separation. Over the range of conditions examined, the reverse or separated flow regions appear to be completely eliminated when the microjets are activated at the appropriate conditions. The parameters examined include the freestream velocity (Reynolds number), the steady momentum coefficient C_μ, and the microjet location. Representative results presented in this paper correspond to a Reynolds number of 2.3×10^6/m; for this case the separation bubble for the uncontrolled flow, more than one-sixth of the ramp length, was completely eliminated with a mass flux input lower than 1% using the microjets. In more recent experiments using even less mass flow through the microjets, we were able to control separation zones that were significantly larger than the results shown herein. Although the mass flux is very low, the microjets produce a rather high steady momentum coefficient, where $C_\mu = 0.29$ for this mass flux. Circumstantial evidence suggests that the physical mechanism behind the control is related to the generation of strong streamwise vorticity produced by the injection of the high-momentum microjet fluid; experiments are planned to obtain more direct evidence. The elimination of separation is accompanied by significant reductions in the velocity fluctuations and the turbulent kinetic energy, another highly desirable feature for most applications. As such, supersonic microjets show considerable promise as simple, adaptable, and effective actuators for controlling flow separation and flow distortion.

Acknowledgments

This study is supported by the NASA Langley Research Center under grants monitored by S. Gorton; the authors are grateful for this support. We thank B. DePriest for his considerable assistance in designing and fabricating the hardware and models. The authors also appreciate the advice of A. Krothapalli and the help of B. Alkislar with the particle image velocimetry measurements.

References

[1]MacMartin, D. G., Verma, A., Murray, R. M., and Paduano, J. D., "Active Control of Integrated Inlet/Compression Systems," Fluids Engineering Div. Summer Meeting, FEDSM2001-18275, June 2001.

[2]Mayer, D. W., Anderson, B. H., and Johnson, T. A., "3D Subsonic Diffuser Design and Analysis," AIAA Paper 98-3418, July 1998.

[3]Wellborn, S. R., Reichert, B. A., and Okiishi, T. H., "Study of Compressible Flow in a Diffusing S-Duct," *Journal of Propulsion and Power*, Vol. 10, No. 5, 1994, pp. 668–675.

[4]Liebeck, R. H., "Design of Blended Wing Body Subsonic Transport," *Journal of Aircraft*, Vol. 41, No. 1, 2004, pp. 10–25.

[5]Rabe, D., Boles, A., and Russler, P., "Influence of Inlet Distortion on Transonic Compressor Blade Loading," AIAA Paper 95-2461, July 1995.

[6]Seifert, A., Darabi, A., and Wygnanski, I., "Delay of Airfoil Stall by Periodic Excitation," *Journal of Aircraft*, Vol. 33, No. 4, 1996, pp. 691–698.

[7]Chang, P. K., *Control of Flow Separation*, Hemisphere and McGraw–Hill, New York, 1970, pp. 154–177.

[8]Gad-el-Hak, M., and Bushnell, D. M., "Separation Control: A Review," *Journal of Fluids Engineering*, Vol. 113, March 1991, pp. 5–30.

[9]Schlichting, H., *Boundary Layer Theory*, 8th ed., Springer-Verlag, Berlin, 2000, pp. 294, 295.

[10]Thomas, F., "Untersuchungen über die Erhöhung des Auftriebes von Tragflügeln mittels Grenzschichtbeeinflussung durch Ausblasen," Dissertation, Inst. of Aerodynamics, Braunschweig, Germany, 1961.

[11]Mokhtarian, F., and Modi, V. J., "Fluid Dynamics of Airfoils with Moving Surface Boundary Layer Control," *Journal of Aircraft*, Vol. 25, No. 2, 1988, pp. 163–169.

[12]Prandtl, L., "Über Flüssigkeitsbewegung bei sehr kleiner Reibung," *Proceedings of Third International Mathematical Congress, Heidelberg, 1904*, Teubner, Leipzig, Germany, 1905, pp. 484–491.

[13]Betz, A., "History of Boundary Layer Control," edited by G. V. Lachmann, *Boundary Layer and Flow Control: Its Principles and Applications*, Vol. 1, Pergamon, New York, 1961, pp. 1–20.

[14]Storms, B. L., and Ross, J. C., "Experimental Study of Lift-Enhancing Tabs on a Two-Element Airfoil," *Journal of Aircraft*, Vol. 32, No. 5, 1995, pp. 1072–1078.

[15]Lin, J. C., "Review of Research on Low Profile Vortex Generators to Control Boundary Layer Separation," *Progress in Aerospace Sciences*, Vol. 38, No. 4, 2002, pp. 389–420.

[16]Zaman, K. B. M. Q., Bar Sever, A., and Mangalam, S. M., "Effect of Acoustic Excitation on the Flow over a Low-Re Airfoil," *Journal of Fluid Mechanics*, Vol. 182, 1987, pp. 127–148.

[17]Ahuja, K. K., Whipkey, R. R., and Jones, G. S., "Control of Turbulent Boundary Layer by Sound," AIAA Paper 83-0726, April 1983.

[18]Amitay, M., Pitt, D., and Glezer, A., "Separation Control in Duct Flows," *Journal of Aircraft*, Vol. 39, No. 4, 2002, pp. 616–620.

[19]Jenkins, L. N., Gorton, S. A., and Anders, S. G., "Flow Control Device Evaluation for an Internal Flow with an Adverse Pressure Gradient," AIAA Paper 2002-0266, Jan. 2002.

[20]Greenblatt, D., and Wygnanski, I. J., "The Control of Flow Separation by Periodic Excitation," *Progress in Aerospace Sciences*, Vol. 36, No. 7, 2000, pp. 487–545.

[21]Alvi, F. S., Elavarsan, R., Shih, C., Garg, G., and Krothapalli, A., "Control of Supersonic Impinging Jet Flows Using Microjets," *AIAA Journal*, Vol. 41, No. 7, 2003, pp. 1347–1355.

[22]Johnston, J. P., and Nishi, M., "Vortex Generator Jets—Means for Flow Separation Control," *AIAA Journal*, Vol. 28, No. 6, 1990, pp. 989–994.

[23]Lou, H., Alvi, F. S., and Shih, C., "A PIV Study of Supersonic Impinging Jet," AIAA Paper 2003-3263, May 2003.

[24]Stratford, B. S., "The Prediction of Separation of Turbulent Boundary Layer," *Journal of Fluid Mechanics*, Vol. 5, 1959, pp. 1–16.

[25]Gustavsson, J., "Experiments on Turbulent Flow Separation," M.S. Thesis, Dept. of Mechanics, Royal Inst. of Technology, Stockholm, Oct. 1998.

[26]Phalnikar, K. A., "An Experimental Study of Free and Impinging Supersonic Microjets," M.S. Thesis, Dept. of Mechanical Engineering, Florida A&M Univ. and Florida State Univ., Tallahassee, FL, May 2001.

[27]Lourenco, L. M., "True Resolution PIV: A Mesh Free Second Order Accurate Algorithm," 10th International Symposium on Laser Techniques Applied to Fluid Mechanics, Lisbon, Paper 13.5, July 2000.

[28]Lourenco, L. M., and Krothapalli, A., "Mesh Free Second Order Algorithm for PIV Processing," *Proceedings of the International Conference on Optical Technology and Image Processing in Fluid, Thermal and Combustion Flows*, Visualization Society of Japan, Yokohama, Japan, 1998, Paper AB079.

[29]Gorton, S. A., Owens, L. R., Jenkins, L. N., Allan, B. G., and Schuster, E. P., "Active Flow Control on a Boundary-Layer-Ingesting Inlet," AIAA Paper 2004-1203, Jan. 2004.

[30]Barberpoulos, A. A., and Garry, K. P., "The Effect of Skewing on the Vorticity Produced by an Air Jet Vortex Generator," *Aeronautical Journal*, Vol. 102, No. 1013, 1998, pp. 171–177.

[31]Tobak, M., and Peake, D. J., "Topology of Three-Dimensional Separated Flows," *Annual Review of Fluid Mechanics*, Vol. 14, Jan. 1982, pp. 61–85.

[32]Lefebvre, A. H., *Gas Turbine Combustion*, 2nd ed., McGraw–Hill, New York, 1983, pp. 110–115.

[33]Alvi, F. S., Lou, H., and Shih, C., "The Role of Streamwise Vorticity in the Control of Impinging Jets," Fluids Engineering Div. Summer Meeting, FEDSM2003-45062, July 2003.

[34]Papamoschou, D., and Hubbard, D. G., "Visual Observations of Supersonic Transverse Jets," *Experiments in Fluids*, Vol. 14, May 1993, pp. 468–471.

[35]Marzouk, Y. M., and Ghoniem, A. F., "Mechanism of Streamwise Vorticity Formation in a Transverse Jet," AIAA Paper 2002-1063, Jan. 2002.

[36]Marzouk, Y. M., and Ghoniem, A. F., "Vorticity Formulation for an Actuated Jet in Crossflow," AIAA Paper 2004-0096, Jan. 2004.

[37]Kumar, V., and Alvi, F. S., "Use of Supersonic Microjets for Active Separation Control in Diffusers," AIAA Paper 2003-4160, June 2003.

W. Dahm
Associate Editor

Color reproductions courtesy of NASA.